Electronic Supplementary Materials for

Dual back interface engineering optimized charge carrier dynamics in $Sb_2(S,Se)_3$ photocathodes for efficient solar hydrogen production

Hafiz Sartaj Aziz[a], Tahir Imran[a], Munir Ahmad[a], Guo-Jie Chen[a], Ping Luo[a], Dong-Lou Ren[b], Bing-Suo Zou[b], Ju-Guang Hu[a], Zheng-Hua Su[a], Pei-Guang Yan[a], Guang-Xing Liang[a], Shuo Chen[a,*]

[a]Shenzhen Key Laboratory of Advanced Thin Films and Applications, Key Laboratory of Optoelectronic Devices and Systems of Ministry of Education and Guangdong Province, College of Physics and Optoelectronic Engineering, Shenzhen University, Shenzhen, 518060, China

[b]State Key Laboratory of Featured Metal Materials and Life-cycle Safety for Composite Structures, Guangxi Key Laboratory of Processing for Non-ferrous Metals and Featured Materials, School of Resources, Environment and Materials, Guangxi University, Nanning, Guangxi 530004, China

[*]Corresponding author: Email: chensh@szu.edu.cn (Prof. Chen)

Note S1. Photoelectrochemical (PEC) measurements

The PEC performance was inspected via a CHI660e electrochemical workstation, which has a standard three-electrode configuration. Where the Ag/AgCl in a saturated KCl solution served as the reference electrode, Pt-wire served as the counter electrode, and an $Sb_2(S,Se)_3$-based photocathode served as the working electrode. The characterization was carried out in a 0.5 M H_2SO_4 electrolyte with 100 mW/cm^2 AM 1.5G simulated sunshine illumination. The Nernst equation can be employed for the conversion of experimental potential ($V_{Ag/AgCl}$) to V_{RHE}:[1]

$$V_{RHE} = V_{Ag/AgCl} + 0.059 \times PH + 0.198 \quad (1)$$

The following equation can be used to acquire the HC-STH conversion efficiency:[2,3]

$$HC - STH\ (\%) = J_{ph} \times \left(V_{RHE} - V_{H^+/H_2}\right)/P_{SUN} \times 100\% \quad (2)$$

where V_{RHE} and J_{ph} represent the working electrode potential vs. the electrolyte with respect to RHE, and the photocurrent density measured with an applied V_{RHE} bias, respectively. V_{H^+}/H_2 denotes the reduction potential of hydrogen at 0 V_{RHE}, and P_{SUN} represents the 100 mW/cm^2 AM 1.5G simulated sunshine illumination intensity.

Note S2. Particle size analysis

Calculating the crystal size using XRD:

Using Scherrer's equation, the average crystallite size (D) of the grains in the thin films was calculated from the broadening of the prominent peaks of the HS1, HS2, and HS3 thin films. Scherrer's equation can be written as:[4]

$$D = (0.9\ \lambda)/\beta cos\theta \quad (3)$$

where λ represents the X-ray wavelength, β signifies the FWHM of the diffraction peaks under consideration, and θ infers the Bragg angle.

Note S3. Energy bandgap analysis

The energy bandgap (E_g) was calculated using the following equations:[2]

$$2\alpha d = ln[(R_{max} - R_{min})/(R - R_{min})) \quad (4)$$

$$\alpha hv = C(hv - E_g)^n \quad (5)$$

where d, R_{max}, R_{min}, α, hv, and C are the thickness of the thin film, critical reflectivity both inside and outside the light absorption region, absorption coefficient, the energy of a photon, and a constant, respectively. For direct band-gap semiconductors, the index n is ≈0.5, while for indirect band-gap semiconductors, it is approximately ≈2.0.

Note S4. Theoretical approach to photocurrent density Analysis

The following formulas were applied to calculate the theoretical photocurrent density of $Sb_2(S,Se)_3$ using the AM 1.5G standard solar spectrum with wavelength-dependent LHE (light harvesting efficiency) (Figure S14a):[5, 6]

$$J_{abs} = \int_{300}^{\lambda_e} \frac{\lambda}{1240} \cdot N_{ph}(\lambda) \times LHE(\lambda) d\lambda \quad (6)$$

$$LHE = 1 - 10^{-A(\lambda)} \quad (7)$$

where J_{abs}, λ, λ_e, $N_{ph}(\lambda)$ and $A(\lambda)$ are the theoretical photocurrent density, wavelength, absorption cut-off wavelength related to band-gap, photon flux (Figure 5a), and absorbance related to wavelength (Figure S14b), respectively.

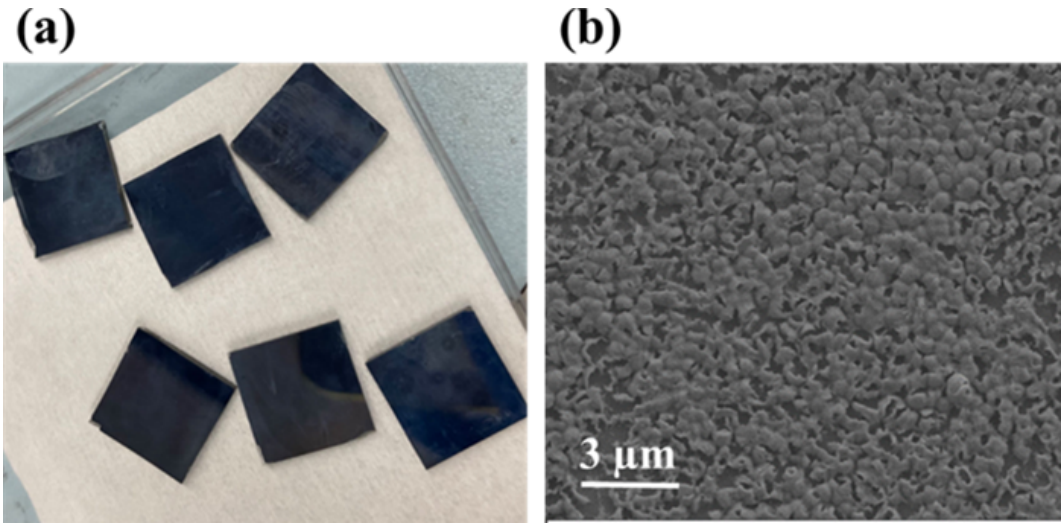

Fig. S1. (a) Inhomogeneous deposition of $Sb_2(S,Se)_3$ thin-film on the pristine Mo substrates prepared by hydrothermal method. (b) SEM picture of an inhomogeneous thin film of $Sb_2(S,Se)_3$ on the pristine Mo substrate.

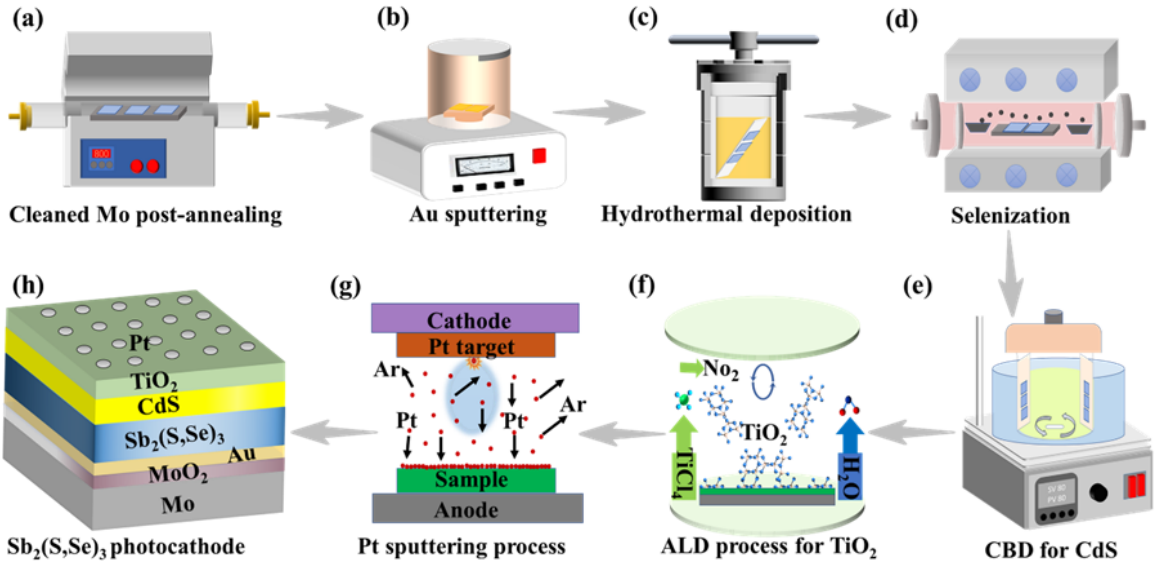

Fig. S2. Schematic diagram illustrating the comprehensive fabrication method of the $Sb_2(S,Se)_3$-based photocathode.

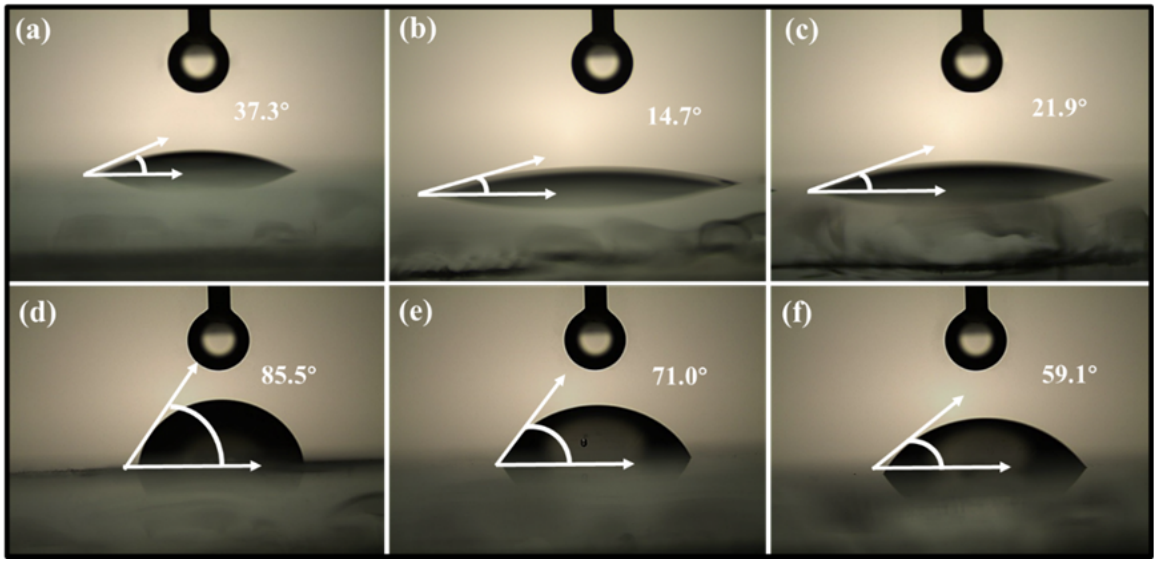

Fig. S3. (a-c) The measured *CA*s (using the glycerol droplet) of pristine Mo, post-annealed Mo at 400°C/15 min, and post-annealed Mo sputtered with Au, respectively. (d-f) the measured CAs of the thin films from HS1, HS2, and HS3 samples.

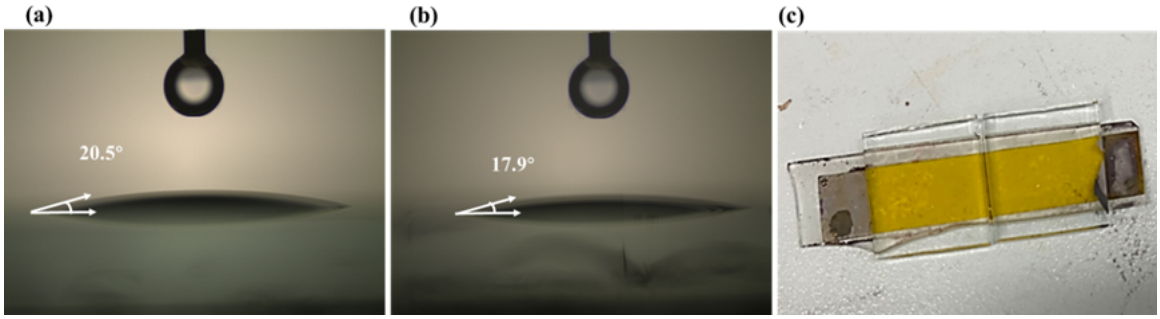

Fig. S4. (a) The measured *CA*s of post-annealed Mo substrates at 200 °C/15 min and (b) 300 °C/15 min, respectively. (c) Mo substrates (annealed at 500 °C/15 min) with $Sb_2(S,Se)_3$ thin films were washed out completely through gradual washing with deionized water after the thin film deposition via hydrothermal method.

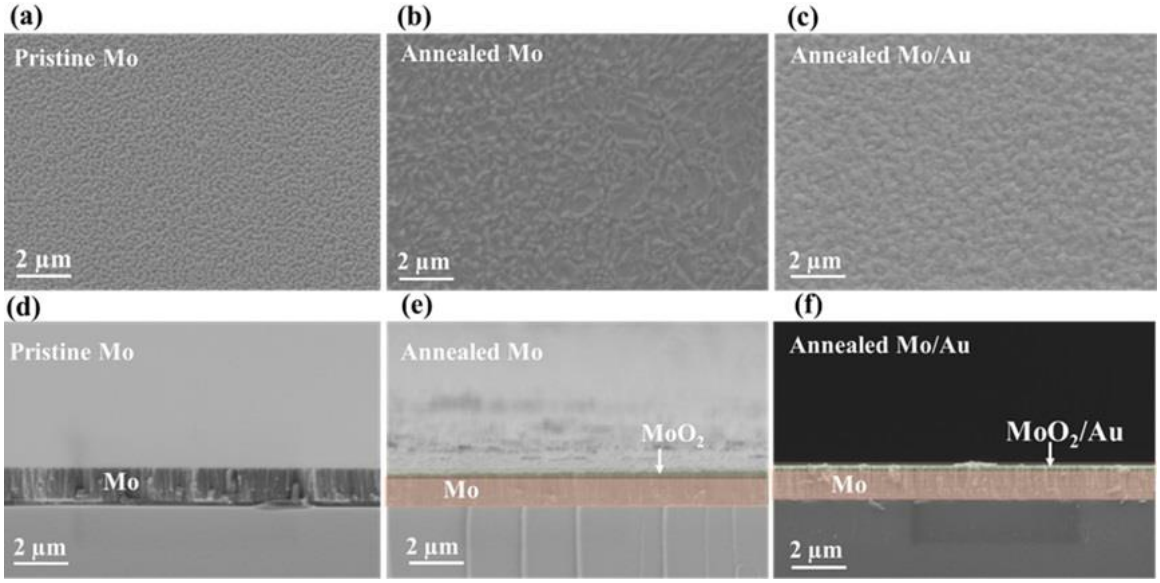

Fig. S5. (a-c) SEM pictures of the surface for the pristine Mo, post-annealed (400°C/15) Mo, and post-annealed Mo sputtered with Au, respectively. (d-f) The corresponding samples' cross-sectional SEM pictures.

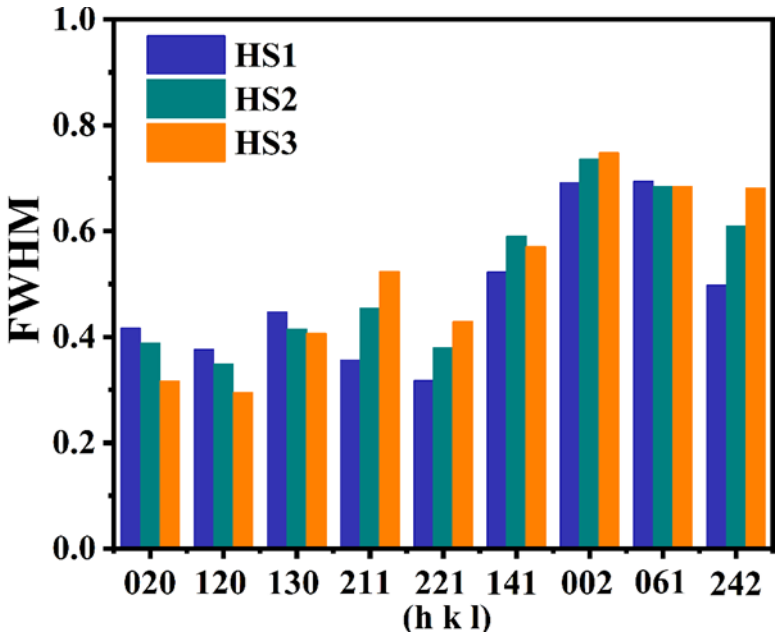

Fig. S6. FWHM of the diffraction peaks of the HS1, HS2, and HS3 thin films.

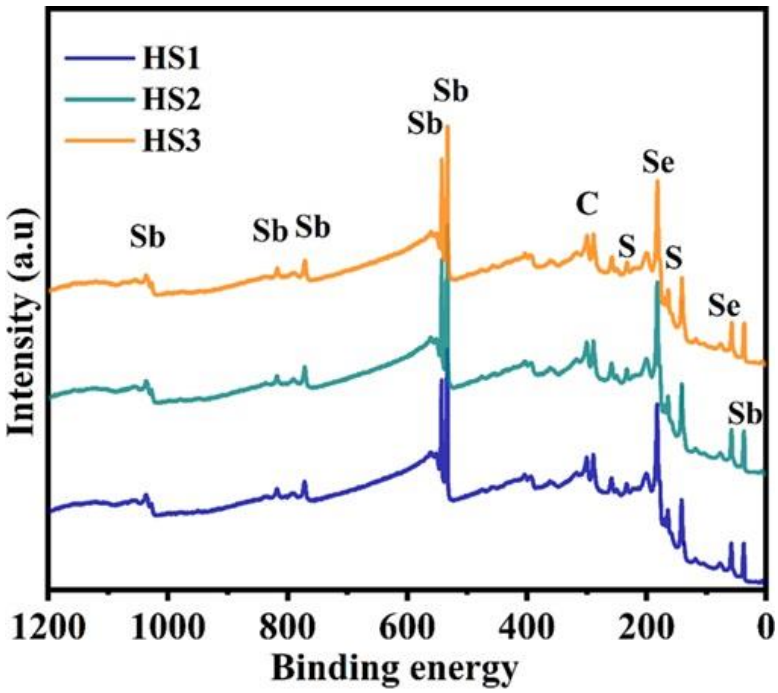

Fig. S7. The total XPS spectra of the HS1, HS2, and HS3, thin films.

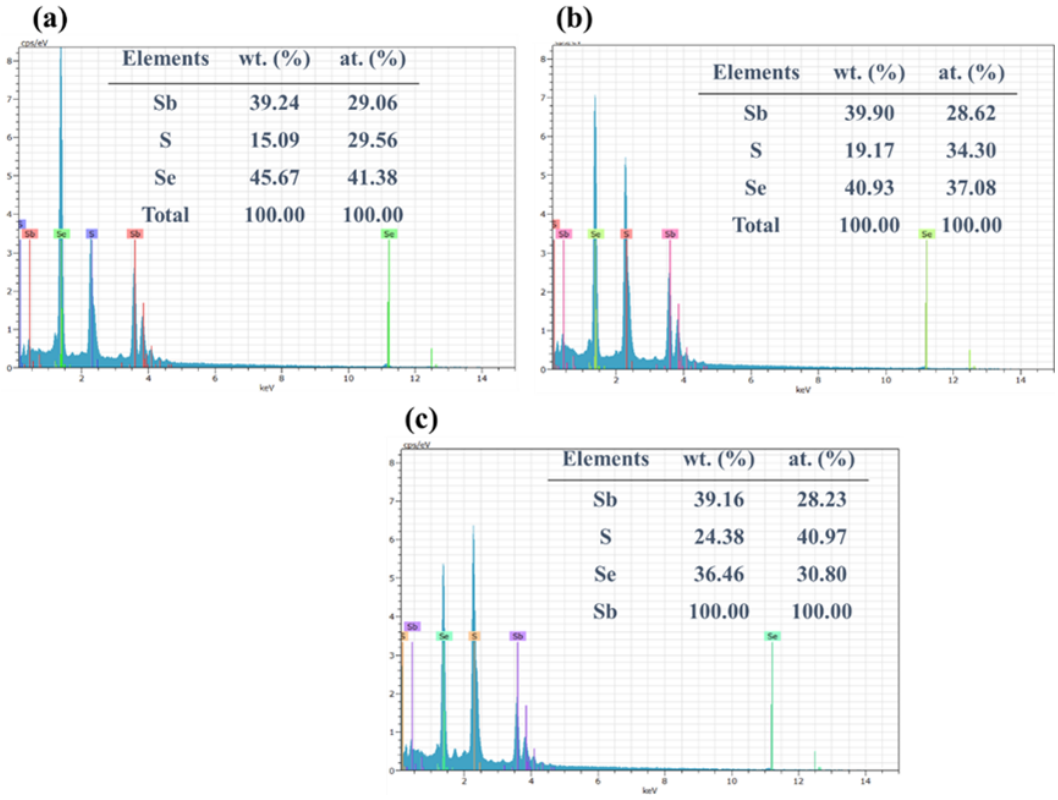

Fig. S8. EDS spectra obtained from (a) HS1, (b) HS2, and (c) HS3 thin films, including their elemental compositions.

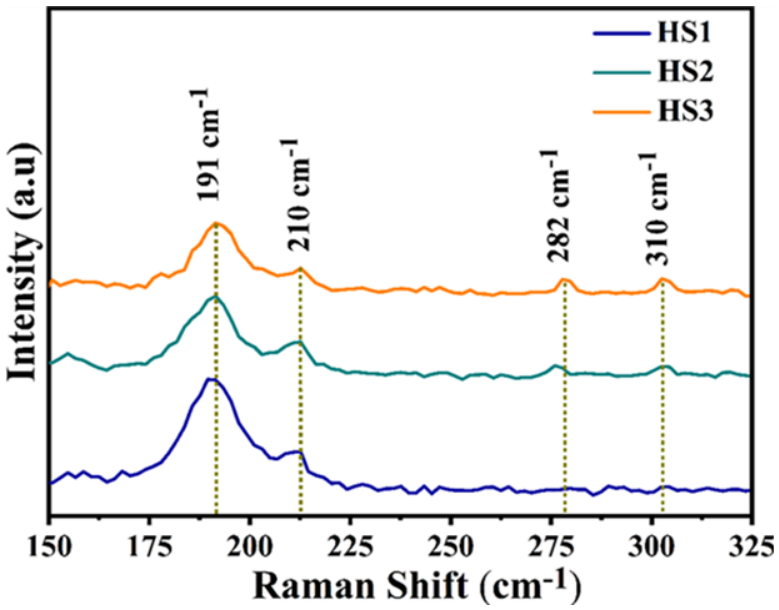

Fig. S9. Raman spectra obtained from (a) HS1, (b) HS2, and (c) HS3 thin films.

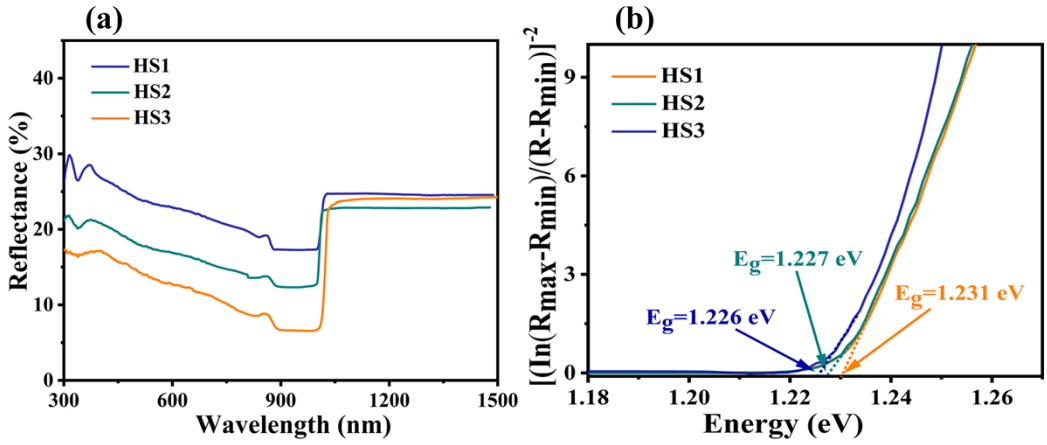

Fig. S10. Optical characterizations of the HS1, HS2, and HS3 thin films (a) Reflectance, (b) plots of $(\ln [R_{max}-R_{min}]/[R-R_{min}])^2$ vs. energy.

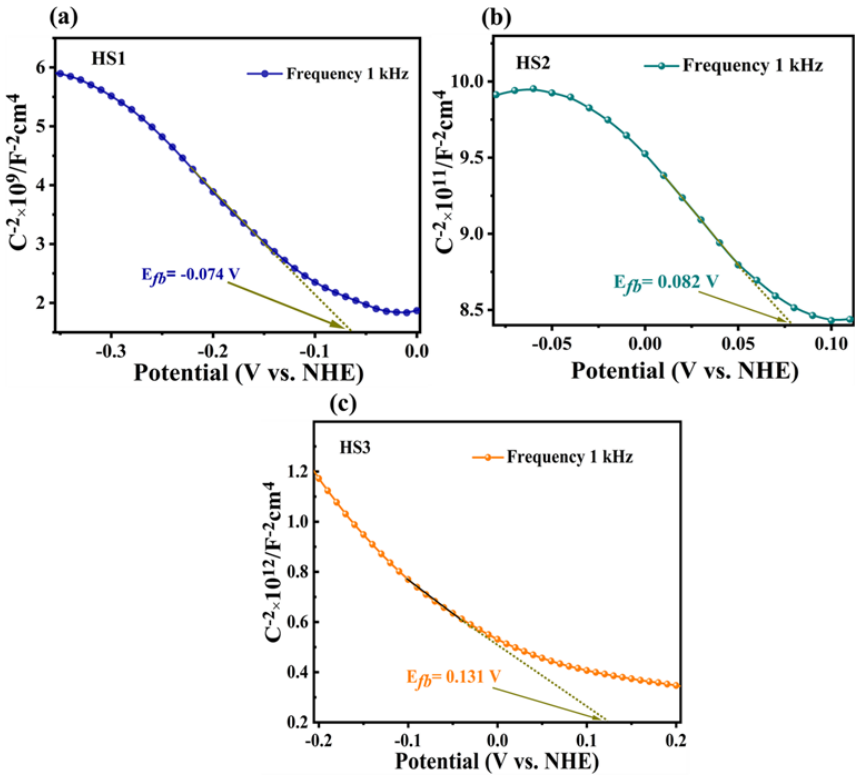

Fig. S11. *M-S* plots of the (a) HS1 (b) HS2, and (c) HS3 thin films at a frequency of 1 kHz.

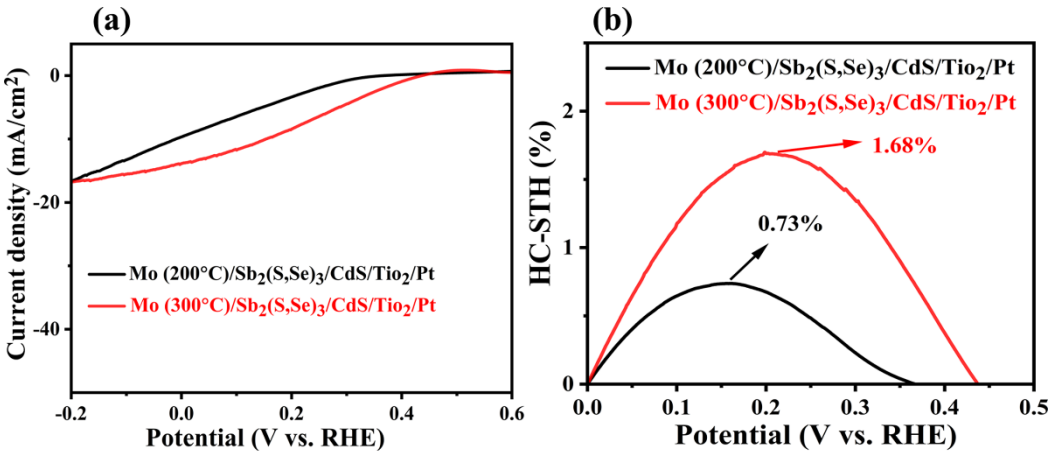

Fig. S12. (a) *J-V* curves of the Mo substrates annealed at different temperatures 200 °C and 300 °C for 15 min, respectively, and (b) the corresponding devices' HC-STH conversion efficiencies.

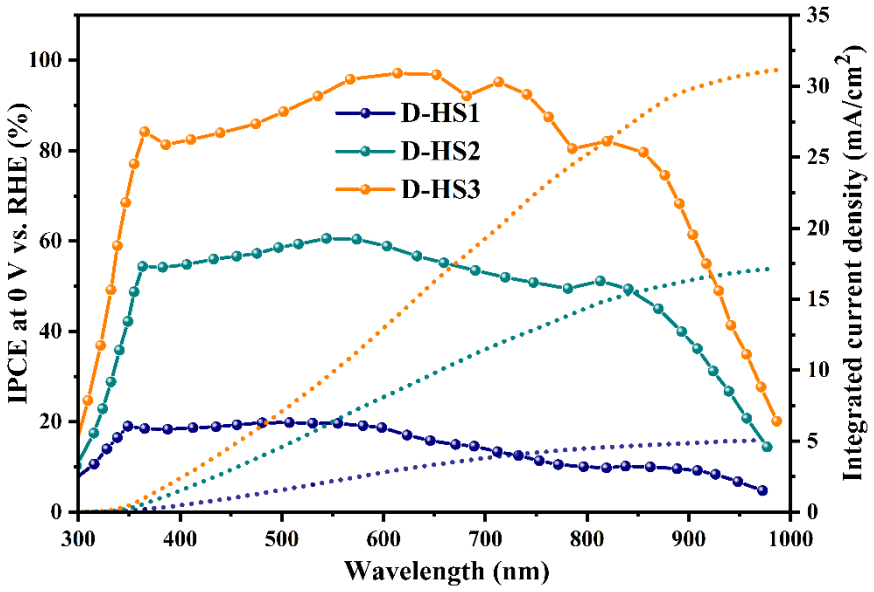

Fig. S13. Wavelength-dependent IPCE at 0 VRHE of the D-HS1, D-HS2, and D-HS3 photocathodes.

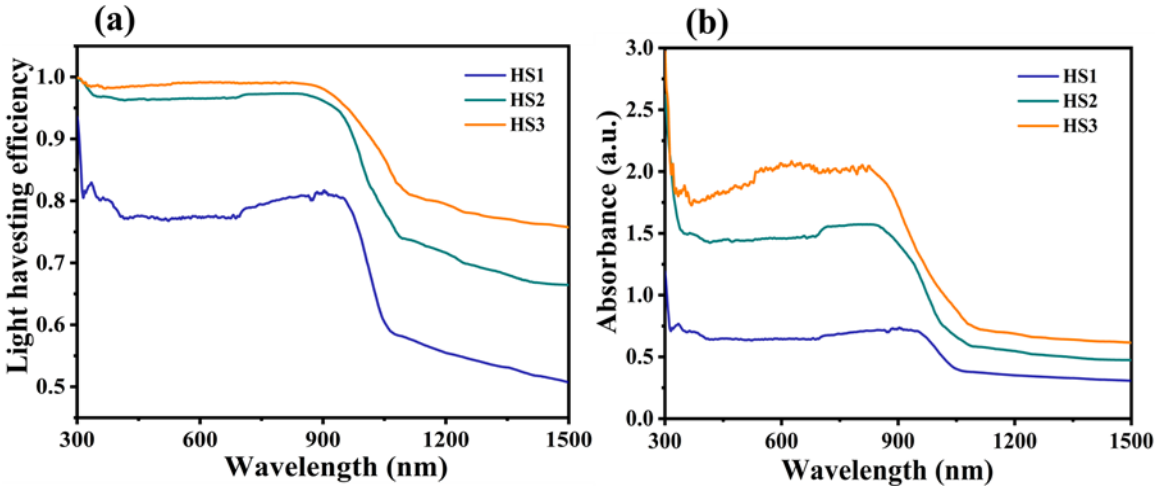

Fig. S14. (a) LHE (light harvesting efficiency) and (b) absorbance of the HS1, HS2, and HS3 thin films.

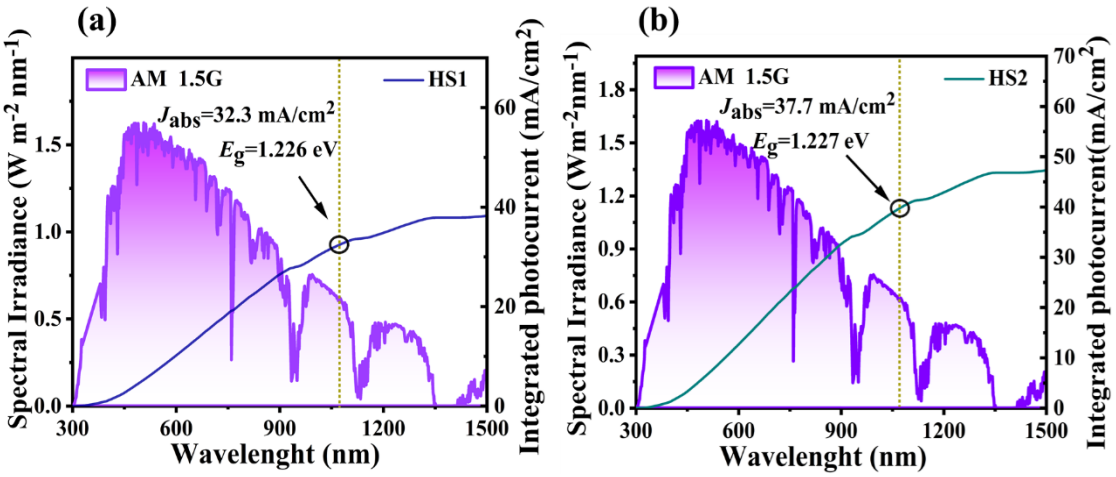

Fig. S15. Energy density flux for the AM 1.5 G standard solar spectrum and integrated photocurrent density of the (a) HS1 and (b) HS2 samples.

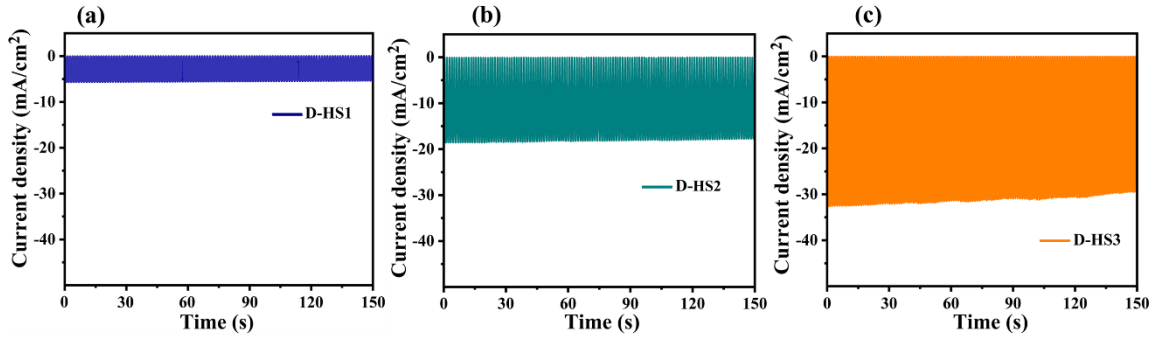

Fig. S16. *J-T* curves of the (a) D-HS1, (b) D-HS2, and (c) D-HS3 photocathodes (at 0 VRHE) under the AM 1.5G simulated sunlight illumination.

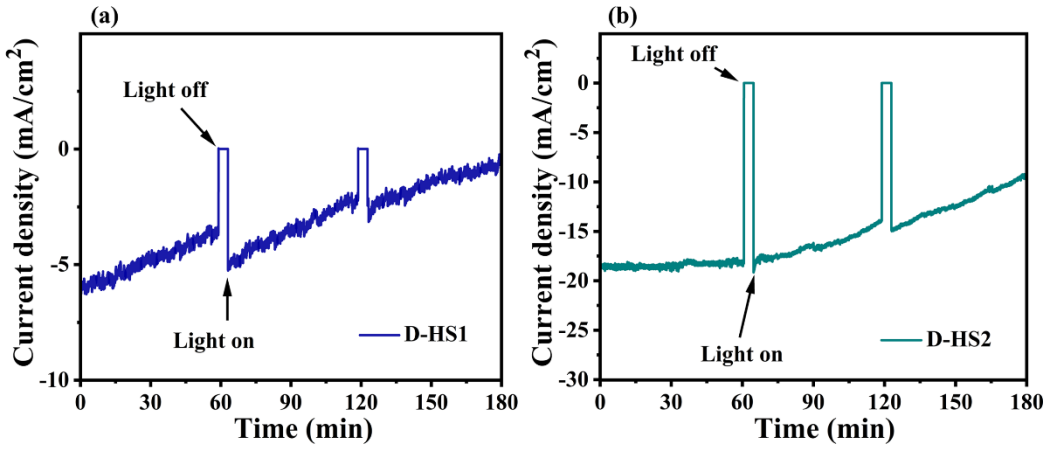

Fig. S17. Photocurrent stability test of the (a) D-HS1 and (b) D-HS2 photocathodes at 0 V_{RHE} for 3 h under illumination.

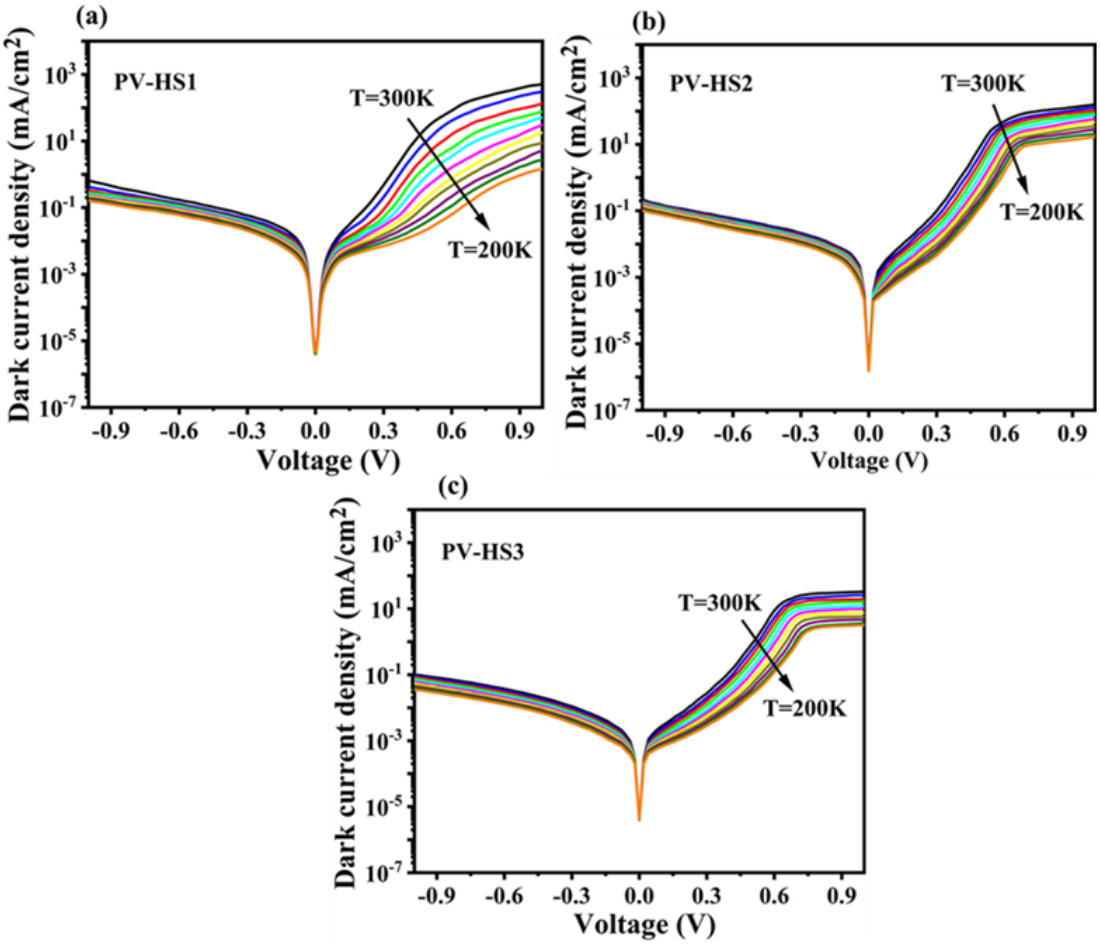

Fig. S18. *J-V-T* plots of the (a) PV-HS1, (b) PV-HS2, and (c) PV-HS3 devices.

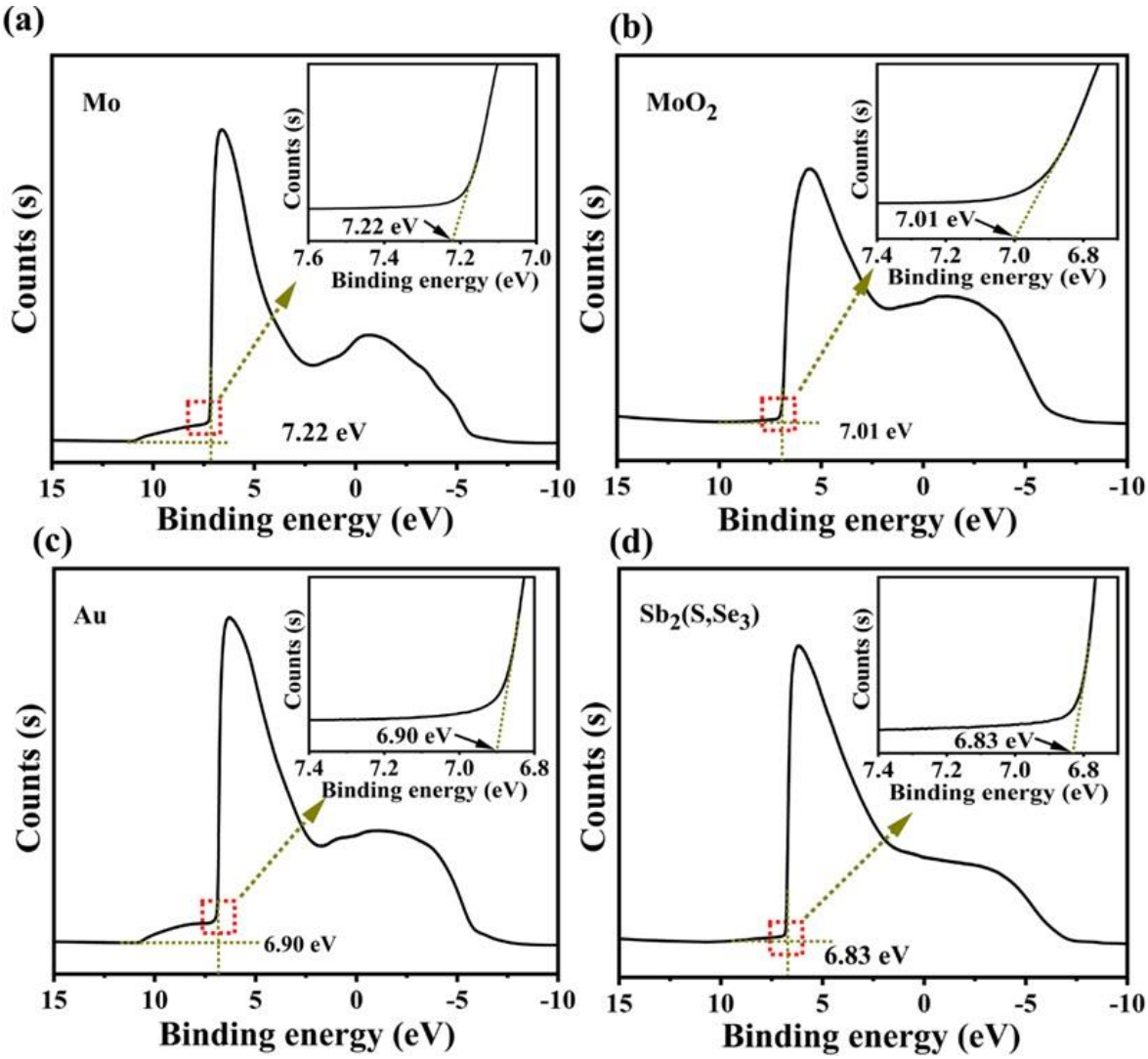

Fig. S19. Schematic diagram illustrating the comprehensive fabrication method of the $Sb_2(S,Se)_3$-based photocathode.

Table S1 Summary of the contact angle, surface roughness, grain size, and elemental composition of thin films from HS1, HS2, and HS3 thin films.

Samples	Contact angle (θ)	Surface roughness (nm)	Grain size (nm)	Sb (%)	S (%)	Se (%)
HS1	87.9º	41.5	16	39.24	15.09	45.67
HS2	73.3º	57.4	19	39.90	19.17	40.93
HS3	61.6º	77.2	15	39.16	24.38	36.46

Table S2 Summary of the XPS results for HS1, HS2, and HS3, thin films.

	HS1		HS2		HS3	
	Chemical bond	Area(P) CPS.eV	Chemical bond	Area(P) CPS.eV	Chemical bond	Area(P) CPS.eV
Sb-Se $3d_{3/2}$	538.41	222923.53	538.13	226034.82	538.11	237882.47
Sb-S $3d_{3/2}$	539.31	103163.83	539. 14	114594.413	539. 17	141924.49
Sb-Se $3d_{5/2}$	529.08	366135.34	529.85	348178.91	529.74	340510.85
Sb-S $3d_{5/2}$	529.85	122624.19	529.68	145494.84	529.87	216964.02
Sb-O	530.96	68379.24	530.23	53229.25	530.38	25038.22

Table S3 The calculated FWHM values of S and Se peaks in HS1, HS2, and HS3, thin films.

	HS1		HS2		HS3	
	Chemical bond	FWHM	Chemical bond	FWHM	Chemical bond	FWHM
S $2p_{1/2}$	162.72	2.03	162.67	1.91	162.88	1.61
S $2p_{3/2}$	160.5	1.52	160.37	1.50	160.34	1.49
Se $3d_{3/2}$	54.62	1.62	54.73	1.74	54.61	2.18
Se $3d_{5/2}$	53.43	1.37	53.68	1.45	53.40	1.95

Table S4 The PEIS fitted parameters for the D-HS1, D-HS2, and D-HS3 photocathodes.

Samples	R_S (Ω)	$R_{HF}(\Omega)$	C_{HF} (F)	$R_{MF}(\Omega)$	C_{MF} (F)
PV-HS1	3.21	1.53	6.22×10^{-4}	33.2	1.21×10^{-3}
PV-HS2	3.51	1.86	2.42×10^{-5}	16.4	1.93×10^{-3}
PV-HS3	3.86	1.37	1.18×10^{-6}	5.04	1.54×10^{-3}

References

1 J. Kim, W. Yang, Y. Oh, H. Lee, S. Lee, H. Shin, J. Kim and J. Moon, *J. Mater. Chem. A*, 2017, **5**, 2180-2187.

2 W. Yang, J. H. Kim, O. S. Hutter, L. J. Phillips, J. Tan, J. Park, H. Lee, J. D. Major, J. S. Lee and J. Moon, *Nat. Commun.*, 2020, **11**, 861.

3 Y. Li, Z. Wang, Y. Zhao, D. Luo, X. Zhang, J. Zhao, Z. Su, S. Chen and G. Liang, *Chin. Chem. Lett.*, 2024**, 35**, 109468.

4 W. J. Liu, Y. H. Chang, C. L. Fern, Y. T. Chen, T. Y. Jhou, P. C. Chiu, S. H. Lin, K. W. Lin and T. H. Wu, *Coatings,* 2021, **11**, 1268.

5 G. Liang, T. Liu, M. Ishaq, Z. Chen, R. Tang, Z. Zheng, Z. Su, P. Fan, X. Zhang and S. Chen, *Chem. Eng. J.*, 2022, **431**, 133359.

6 T. Zhou, S. Chen, J. Wang, Y. Zhang, J. Li, J. Bai and B. Zhou, *Chem. Eng. J.*, 2021, **403**, 126350.